A Quantum-mechanical Study of the Binding Pocket of Proteorhodopsin: Absorption and Vibrational Spectra Modulated by Analogue Chromophores

F. Buda[a*], T. Keijer[a], S. Ganapathy[a], W.J. de Grip[a,b*]

[a] Leiden University, Leiden Institute of Chemistry, Einsteinweg 55, 2300 RA, Leiden, The Netherlands

[b] Radboud University Medical Center, Radboud Institute for Molecular Life Sciences, P.O. Box 9101, 6500 HB Nijmegen, The Netherlands

Corresponding authors email: f.buda@chem.leidenuniv.nl; Wim.deGrip@radboudumc.nl

Abstract

Proteorhodopsin is a light-driven proton pumping membrane protein related to bacteriorhodopsin. It contains an all-*trans* retinal A1 chromophore covalently bound to a lysine residue via a protonated Schiff base. In this study we exploited density functional theory (DFT) calculations to investigate the retinal binding pocket in the dark state and after mimicking photoisomerization. The model of the binding pocket is constructed incrementally by adding the residues near the retinal that are necessary to ensure a stable protonated Schiff base. The presence of a few water molecules near the Schiff base turns out to be an essential feature of the model. The absorption properties are then studied using time-dependent DFT (TDDFT) and compared to experimental data to further validate the structural model and to assess the accuracy of the computational setting. It is shown that TDDFT is able to reproduce the main absorption peak accurately and to quantitatively determine the spectral shift induced by substituting the native all-*trans* retinal A1 chromophore with different retinal analogues. Moreover, *ab-initio* molecular dynamics simulations are performed to investigate the vibrational spectra of our models before and after isomerization. Specific differences in the vibrational spectra are identified that provide further insight in experimental FTIR difference spectra.

Introduction

Proteorhodopsin (PR) is a member of an abundant family of photoactive transmembrane proteins with a retinal chromophore bound to a conserved lysine.[1] First discovered in marine bacteria of the SAR86 group, it acts as a proton pump similar to the well-studied bacteriorhodopsin (BR).[2] Since their discovery, many different variants have been found and characterized.[3] For PR two variants have been discovered, a green absorbing one (denoted GPR, λ_{max} ~ 520 nm) and a blue absorbing one (denoted BPR, λ_{max} ~ 490 nm).[1] It is well known that the spectral features of the retinylidene chromophore are strongly affected by the protein environment and considerable tuning of the absorption maximum can be obtained by mutagenesis.[4,5] Spectral modulation can also be achieved by changing the electronic and conformational properties of the retinal itself. Recently, Ganapathy et al. used a combination of retinal analogues with directed mutations in the retinal binding pocket to modulate the absorbance properties and proton pump activity of PR.[6,7]

GPR presents a photocycle very similar to BR, with a first intermediate after photoisomerization, named *K*, which contains the 13-*cis* configuration of the chromophore. This first step occurs within a time scale of a few ps and is followed by much slower structural changes in the protein leading to a deprotonation of the Schiff base in a µs time scale (state *M*). Since no crystallographic structure is currently available for GPR, homology models have been generated based on the structure of xanthorhodopsin (XR) and BPR.[6,8,9] A characteristic feature of the protonated Schiff base (PSB) binding pocket is the complex counterion formed by the residues Asp97 and Asp227. Moreover, the presence of water molecules in the vicinity of the PSB has also been indicated by previous investigations, although the exact number and position is difficult to establish. [10,11]

In this study we build and investigate a model of the retinal binding pocket in GPR using Density Functional Theory (DFT) calculations and *ab-initio* molecular dynamics simulations. This model is first validated on the basis of the PSB stability in the dark state. It is found that an essential feature of the binding pocket is the presence of a hydrogen bonding network involving three water molecules in the near proximity of the PSB. These water molecules stabilize the counterion and provide a channel for proton rearrangement during the photocycle. The model is further validated by comparing the computed absorption spectrum with available experimental data. This study is extended to include retinal analogues that have been shown to strongly modulate the spectral properties and proton pump activity of GPR (Figure 1).[7] Models for the early *K* intermediates are also studied and vibrational properties are compared with available FTIR difference spectra. The overall very good agreement with experimental data and the ability to closely reproduce spectral trends underline the predictive power of DFT-based simulations and their role as a complementary tool to experimental studies.

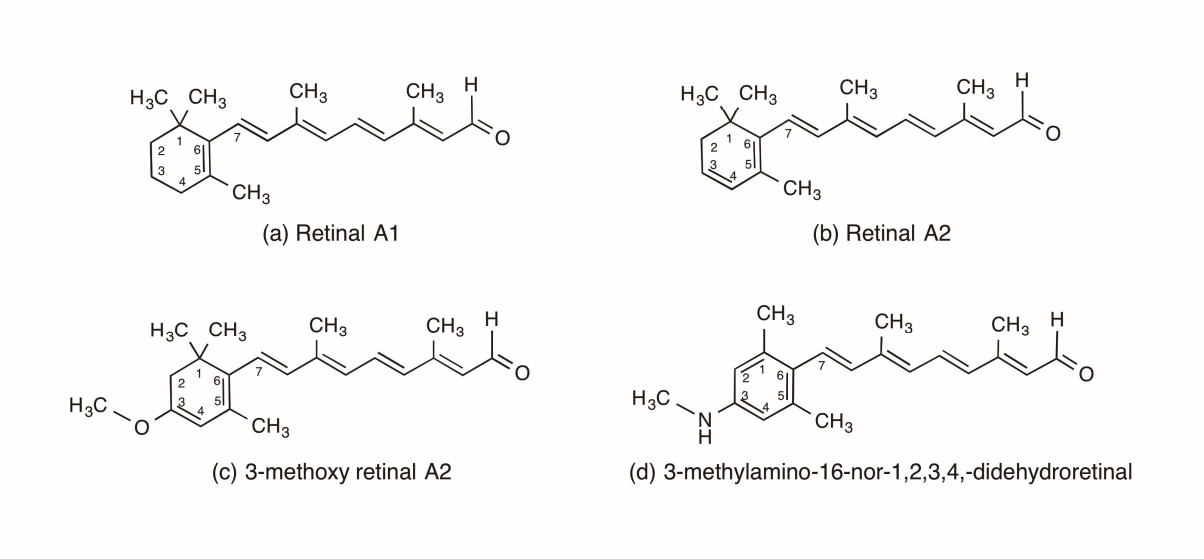

Figure 1. Chemical structure of the all-*trans* isomers of retinal A1 and the analogues investigated in this work. (a) Retinal A1, the chromophore present in the native PR. (b) Retinal A2, containing an additional double bond between C3 and C4. (c) 3-methoxy retinal A2 (called 3MA2 in the text). (d) 3-methylamino-16-nor-1,2,3,4,-didehydroretinal (called MMA in the text), containing an additional double bond between C1 and C2.

Computational methods and details

All geometry optimizations and time-dependent density functional theory (TDDFT) calculations are performed using the Amsterdam Density Functional (ADF) software package.[12–14] For the geometry optimizations, the PBE generalized gradient approximation (GGA) for the exchange-correlation functional is used.[15] Van der Waals (vdW) interactions are accounted for by using the Grimme3 BJDAMP dispersion correction.[16] The Slater type orbitals basis set TZP (triple zeta with one polarization function) with a small frozen core approximation is used for all the calculations. Linear response TDDFT excited state calculations are performed with the hybrid B3LYP functional[17] combined with the same TZP basis set and vdW corrections. Additional TDDFT calculations are performed with the long-range corrected functional CAM-B3LYP using the same basis set and no frozen core.[18,19]

Ab-initio molecular dynamics (AIMD) simulations are performed using the Car-Parrinello Molecular Dynamics (CPMD) package.[20,21] The same PBE functional is employed also for the AIMD simulations. The Kohn-Sham orbitals are expanded in a plane wave basis set with a cut-off energy of 70 Ry. Dispersion-corrected atom-centered pseudopotentials (DCACP) are used for all atomic species.[22] The time-step is set to 4 a.u. The optimized geometries obtained with the ADF calculations are used as initial coordinates for the AIMD. Starting with zero velocities, the ions are smoothly thermally equilibrated at 300 K using a Nosé-Hoover thermostat, [23,24] and the system is then evolved for about 2 ps. The MD box has an orthorhombic symmetry with lattice parameters of 18.5 Å, 17.5 Å, 24.5 Å, respectively and is treated as an isolated system where the Poisson equation is solved using the Hockney method.[25]

The vibrational density of states (VDOS) is obtained from the AIMD trajectories by taking the Fourier transform of the velocity autocorrelation functions. This can be done considering all the atoms in the system, or by selecting specific atoms or geometrical parameters. In this way, specific vibrational modes can be easily identified and compared with experimental infrared absorption bands. In particular, by examining the difference between the spectra obtained for the all-*trans* and 13-*cis* conformation of the chromophore, we provide evidence of changes in vibrational modes for relevant parts of the system after photo-isomerization.

Results and Discussion

Models investigated: Characterization and validation

The initial Cartesian coordinates for all the models considered in this study are extracted from the homology structure of GPR derived in previous work.[6] This homology structure shows excellent conformity with a recently published crystal structure for BPR (PDB code 4KNF).[9] First we consider a model for the GPR active site with the native retinal A1 chromophore in the all-*trans* conformation (see Figure 1a). The model is built in an incremental way starting from a minimal model and by progressively adding residues in close proximity of the retinal PSB: in this way we can establish the essential elements in the binding pocket that contribute to the structural stability and optical absorption properties of the system.

The retinal is covalently bound through a protonated Schiff base to a lysine residue (Lys231) that is included in our model up to the γ-C position. This carbon is replaced by a methyl group (see Figure 2). To mimic the mechanical constraints imposed by the protein environment, the coordinates of the carbon atom of the methyl group used to terminate the chain of this residue is fixed during the geometry optimization and the AIMD simulations. A similar strategy and constraint is used to terminate all the other residues included in the model. Moreover, the carbon atoms of the methyl groups on the β-ionone ring of the retinal are also kept fixed, in view of evidence that their mobility is strongly constrained by the protein binding pocket.[26–29]

The counterion is of course an important element of the model, especially if we want to accurately describe the optical response of the system. It is well known that the PSB-retinal is highly polarizable and that its structural and electronic properties are strongly sensitive to the type and position of the counterion.[30,31] In GPR, the main counterion is Asp97 (see Figure 2), which is found in close proximity to the PSB and acts as the primary proton acceptor in the formation of the M state.[1]

A geometry optimization with the above-mentioned constraints of a minimal model, including the retinal in the presence of only this counterion (PSB-Ret-A1 + Lys231 + Asp97) leads to a proton transfer from the Schiff base to the counterion. Clearly, this deprotonated Schiff-base does not correspond to the expected result for the initial GPR dark state. To check if this result is due to the inaccuracy in the GGA description of the proton transfer reaction,[32] we have performed an additional test with the more accurate B3LYP functional. This further test results again in the same proton transfer with very small differences between the two geometries optimized at the PBE and B3LYP level of theory. Therefore, we can conclude that this minimal model is still missing crucial elements of the binding pocket.

It has been shown in the literature that the pK_a value of Asp97 is lowered because of the nearby residue His75.[33] This histidine residue is protonated in the dark-state, thus adding a net positive charge in the binding pocket. Another important residue that contributes to the complex counterion in GPR is the negatively charged Asp227, which plays a critical role in the photocycle, as it facilitates the reprotonation reaction.[34] By including Asp227 and His75 in the model (see Figure 2), we obtain an overall neutral system. However, geometry optimization of the model including the Asp227, Asp97, and His75 residues results again in an unrealistic proton transfer, in this case from His75 to Asp97.

The next step in generating a more realistic model requires the formation of a hydrogen bonding network that can play the double role of stabilizing the initial (dark) protonation state and facilitating the proton transport mechanism during the photocycle. Several experimental and computational studies have recently pointed out the importance of water molecules in retinal binding pockets that appear to be strongly bound, and contribute to the overall stability of the protein structure and to the spectral tuning.[10,11,35–37] Moreover, MD simulations in aqueous environment show that water is able to solvate a large portion of the interior of PR all the way to the active site.[38] Therefore, we have incrementally added three water molecules in the active site and optimized their position while keeping the other residues in the model fixed. Also a tyrosine residue Tyr200, which is hydrogen bonded to Asp227, is included in the model: in BPR its alcohol group is in close proximity to the Asp227 and enhances the hydrogen-bonding network.[9] To minimize the additional atoms and consequent computational costs in the model, the hydrogen-bonding properties of the phenol are recreated by substituting the entire conjugated system by just the hydroxy-carbon element, effectively introducing a methanol molecule in its place. The geometry optimization of the whole system leads to the structure shown in Figure 2, where the hydrogen bond network can be visualized. The PSB is now stable and no unnatural structural rearrangement is observed. This model of the binding pocket now includes 111 atoms and constitutes a quantum-mechanical model that can be confidently used for future QM/MM embedding studies.

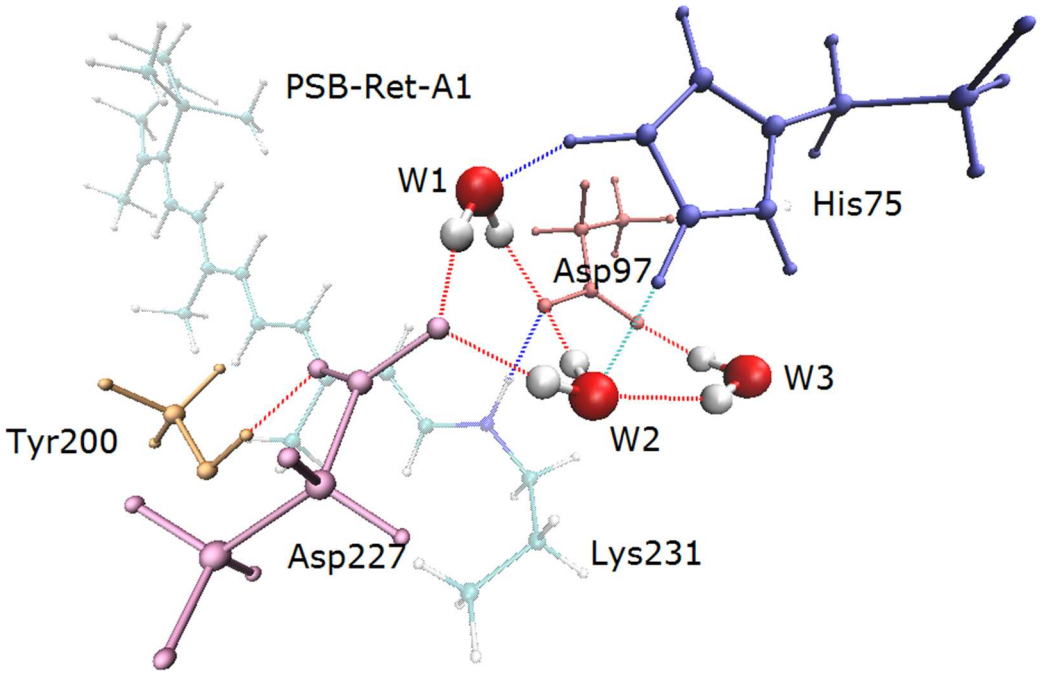

Figure 2. Optimized geometry of the model of the binding pocket of native GPR investigated in this work. The chromophore all-*trans* retinal A1 (light blue) is covalently bound to Lys231 via a protonated Schiff base (PSB-Ret-A1). The complex counterion of the PSB includes the negatively charged Asp97 and Asp227. The net charge in the close proximity of the chromophore is equal to zero because of the presence of the protonated histidine His75. The protonation state in the dark state is stabilized by the presence of a hydrogen bonding network including Tyr200 (hydrogen bonded to Asp227) and three water molecules (W1, W2, and W3). Dotted lines indicate hydrogen bonding interactions.

The binding pocket model constructed for the native all-*trans* A1 chromophore also serves as a basis to construct the 13-*cis* photoproduct. In this study we are not aiming to simulate the photoisomerization process. This is projected for future research. Instead, here we take a more pragmatic approach: the isomerized state is generated by starting from the optimized all-*trans* chromophore and just rearranging the atoms near the C13=C14 isomerizable bond into a 13-*cis* conformation by a "bicycle-pedal" type of motion:[39] this rearrangement is done while keeping fixed the C atoms of all the methyl groups in the model and all the atoms in the residues included in the binding pocket. The modified structure, now in the 13-*cis* conformation, is again optimized except for the position of the C atoms of all the methyl groups as described for the all-*trans* geometry. This procedure is justified considering that the protein structure is unlikely to vary considerably in the very short sub-picosecond time scale in which the photoisomerization takes place. The overlay of the optimized all-*trans* and 13-*cis* models shows that the atomic displacements are overall small (see Figure S1 in the Supporting Information).

Table 1. Comparison of relevant hydrogen bonding distances (Å) before (all-*trans*) and after (13-*cis*) isomerization in the GPR model with the native PSB-Ret-A1 chromophore. The labels in brackets denote the water molecule or the residue number considered (see also Figure 2).

	All-*trans*	13-*cis*
N(PSB)-O(97)	2.72	2.68
O (W1)-O (W2)	3.66	3.76
O (W1)-O (W3)	5.49	5.87
O (W2)-O (W3)	3.00	3.98
O (W1)-O(97)	2.81	2.87
O (W3)-O(97)	2.74	2.64
O (W1)-O(227)	2.66	2.61
O (W2)-O(227)	2.69	2.76
N(His)-O (W3)	2.76	2.68

The total energy of the optimized 13-*cis* model is about 10 kcal mol^{-1} higher than the all-*trans,* which is quite realistic considering the about 12 kcal mol^{-1} stored in the first photoproduct of bacteriorhodopsin.[40] The main structural modifications due to this arranged isomerization are visible in the hydrogen bonding distances collected in Table 1. It can be noticed that the hydrogen bond between the PSB nitrogen and the oxygen of Asp97 becomes stronger in the 13-*cis* conformation, possibly facilitating the proton transfer step. Also, the water molecules respond to the isomerization by slightly modifying their hydrogen bonding distances. In particular, the distance between the water W2 and the water W3 increases considerably upon photoisomerization, thus weakening their hydrogen bond interaction. At the same time the water W3 strengthens the hydrogen bond interaction with the Asp97 and His75 residues.

This binding pocket model was further used to build the models with the retinal analogues considered in this work (Figure 1). The β-ionone ring of the retinal is modified accordingly and the geometry re-optimized by fixing only the carbon atoms of the methyl groups on the β-ionone ring, of the methyl groups on C9 and C13, and of the methyl groups terminating Lys231, Asp227, Tyr200, His75, and Asp97. Only in the case of the MMA analogue, the position of the single methyl group on the C1 position is optimized as well, due to absence of data on this steric environment. The final structures are highly similar to the native system, in the sense that the Schiff-base, the residues and the water molecules do not show significant rearrangements. Only the bonding pattern in the ring element is of course changed in the retinal analogues. Moreover, the bond length alternation (BLA) is also affected by the extended conjugation due to the ring modifications. The Cartesian coordinates of the optimized geometries for all the investigated models are available in the Supporting Information.

Absorption spectra of native and analogue pigments

The optimized structures of the different models, both in the all-*trans* and 13-*cis* configuration are used to calculate the absorption spectrum with TDDFT. The first 30 singlet excitations are calculated for all the models. The computed spectra together with the experimental ones are shown in the Supporting Information (Figure S2). The results for the first excitation energies are collected in Table 2 and compared with available experimental data for the first absorption maximum (λ_{max}).[7] TDDFT at the B3LYP/TZP level of theory is clearly able to correctly reproduce the trend of the experimental data. Moreover, the agreement between the predicted excitation energy and the experimental data is remarkable. For the native all-*trans* A1 case, the deviation from the experimental λ_{max} is only about 10 nm (0.04 eV), well within the typical accuracy expected using the B3LYP functional. This result

constitutes a further strong validation of the structural model for the binding pocket discussed above (Figure 2).

Table 2. TDDFT excitation energies and corresponding oscillator strength computed at the B3LYP/TZP level of theory. Only the first dominant excitations are here presented. The experimental data are from ref. [7] H stands for HOMO, L for LUMO. The computed average BLA is shown in the last column.

Retinal analogue (configuration)	Excitation energy (eV) (oscillator strength) (orbital transitions)	Excitation energy (nm)	Experiment λ_{max} (nm)	Average BLA (pm)
GPR+A1 (all-*trans*)	2.43 (0.86) (H→L & H-1 →L) 2.48 (0.75) (H-1 →L & H →L)	510.7 499.2	520	6.82
GPR+A1 (13-*cis*)	2.30 (0.71) (H→L & H-1 →L) 2.53 (0.90) (H-2→L & H→L & H-1 →L)	539.0 489.9		
GPR+A2 (all-*trans*)	2.24 (1.63) (H→L)	553.5	552	6.04
GPR+A2 (13-*cis*)	2.24 (1.49) (H→L)	552.5		
GPR+MMA (all-*trans*)	2.18 (1.64) (H→L)	567.6	567	5.94
GPR+MMA (13-*cis*)	2.19 (1.61) (H→L)	566.1		
GPR+3MA2 (all-*trans*)	2.16 (1.81) (H→L)	573.3	585	5.30
GPR+3MA2 (13-*cis*)	2.16 (1.74) (H→L)	573.5		

The predicted excitation energies for the models with the A2 and MMA retinal analogues even more accurately reproduce the experimental spectral data. The deviation between theory and experiment for the 3MA2 analogue is about 0.04 eV, similarly to the A1 case.

Because of the partial charge transfer character of the excitation, it has been shown that the long-range corrected CAM-B3LYP functional is more accurate than B3LYP when considering the potential

energy curve along the photo-isomerization torsional angle.[41] In this work, we only consider the excitation energies at the stable intermediates, for which the B3LYP functional should, and herein does, provide reliable results. Nevertheless, calculations have also been performed with the CAM-B3LYP functional for all the analogues in the all-*trans* conformation for comparison. The results are reported in the Supporting Information, Table S1. The outcome is that CAM-B3LYP also yields the correct trend in comparison with experimental data. The absolute value of the first excitation energy is however blue-shifted by about 0.2 – 0.3 eV with respect to the B3LYP results and to the experimental data.

A strong linear correlation (correlation coefficient R^2=0.97) is found between the first excitation energy and the average BLA in different analogues (see last column in Table 2). The average BLA is computed by considering the average bond length difference between single and double bonds from C6-C7 up to C15-N.[42,43]

In Table 2, one can also notice that the major absorption peak is associated in most cases with a HOMO to LUMO transition. However, in the all-*trans* A1 model, there are two closely spaced excitations with comparable oscillator strength originating from HOMO-1 to LUMO and HOMO to LUMO transitions. In the 13-*cis* model, the first excitation is red-shifted from 510 to 539 nm, while the second is slightly blue-shifted from 499 to 490 nm. These spectral features computed for the 13-*cis* A1 retinal model correlate well with experimental data obtained by Lenz et al using ultrafast transient absorption spectroscopy in the time scale of 150 – 280 fs (see Figure 3).[44] Our computed spectrum is indeed based upon a binding pocket that has been optimized only in the near proximity of the retinal. It does not include any subsequent relaxation of the protein environment that takes place on a longer time scale of 10-30 ps, in which the absorption band around 580 nm of the *K*-state fully develops.[44,45] Thus, we can conclude that our 13-*cis* model is more representative of an early intermediate formed in the sub-picosecond time scale, rather than of the fully relaxed *K*-state intermediate. This result is a further confirmation of the strength of our computational approach.

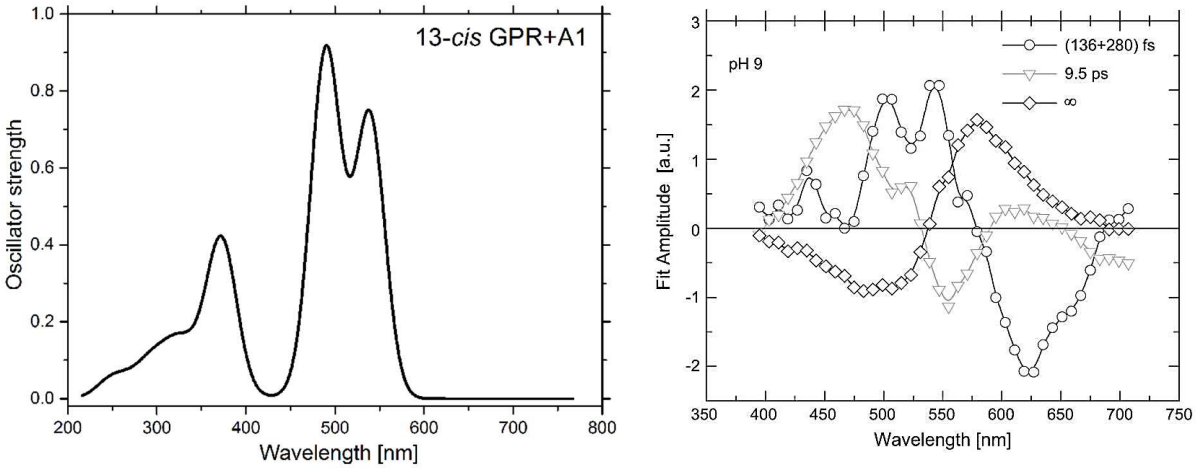

Figure 3. Right panel: Transient absorption data, represented with permission from ref. [44] Left panel: TDDFT computed absorption spectrum for the 13-*cis* GPR+A1 model.

Ab initio molecular dynamics and vibrational spectra

AIMD simulations have been performed for the GPR model with the native retinal A1 both in the all-*trans* and in the 13-*cis* conformations. The analysis of the 2 ps trajectories provides information on characteristic changes in the vibrational spectrum induced by the photoisomerization. These results can be compared to experimental FTIR difference spectra. In Figure 4, we report the difference between the computed VDOS for the all-*trans* and the 13-*cis* models obtained by including only the trajectory of the four carbon atoms C12, C13, C14, and C15 around the isomerizable bond. The most intense features are observed in the region between 1050 cm^{-1} and 1250 cm^{-1} corresponding to the complex retinal fingerprint region. These changes correlate quite well with experimental FTIR data. [46,47] For instance, the peak at 854 cm^{-1}, present in the all-*trans* model but hardly detectable in the 13-*cis* case, probably corresponds to the C14-H wag vibration,[48] which is downshifted and weaker in the 13-*cis* isomer.[49]

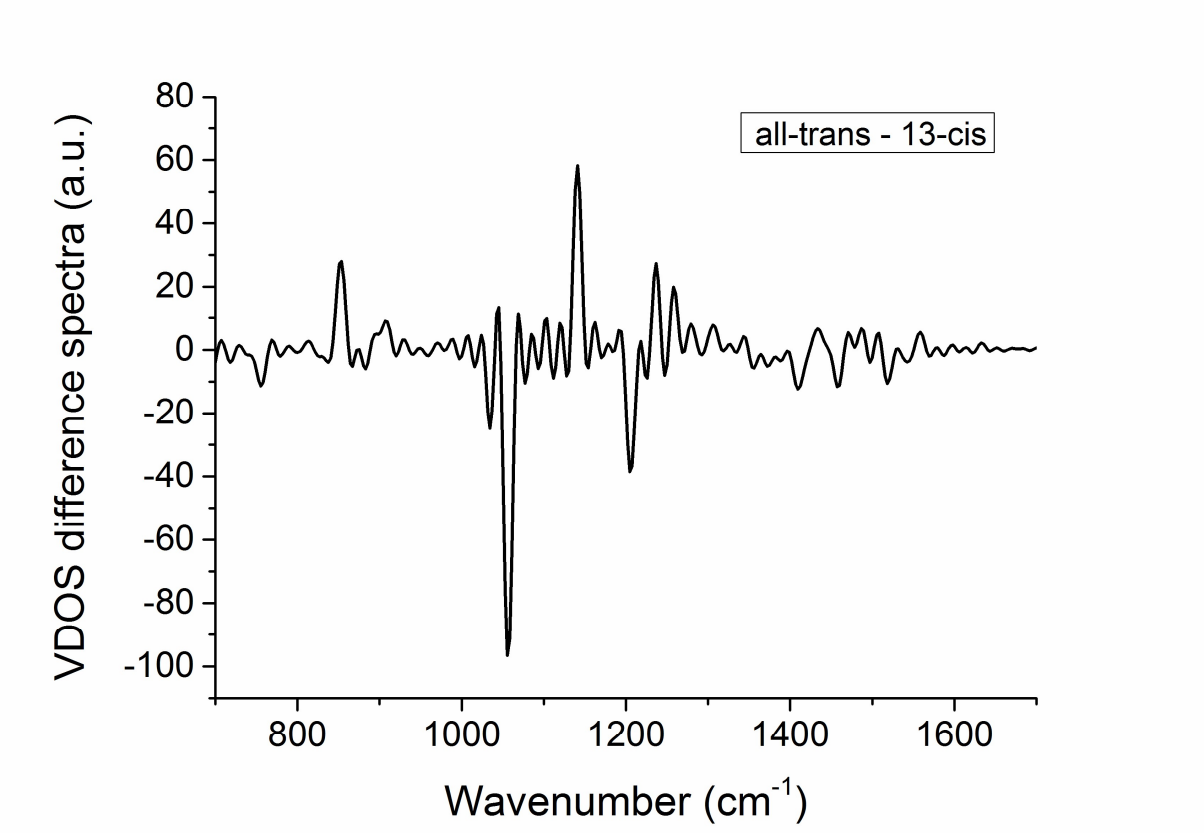

Figure 4: VDOS difference spectrum calculated by subtracting the 13-*cis* configuration from the all-*trans* configuration for our model of the native retinal A1 binding pocket. The spectra are obtained by selecting only the trajectory of the C12, C13, C14, and C15 carbon atoms.

It is interesting to analyse the dynamics of the N-H bond in the PSB before and after isomerization. The vibrational analysis of the trajectory of these two atoms shows a clear shift in the position of the stretching band peak, which moves from 2720 cm^{-1} in the all-*trans* to 2550 cm^{-1} in the 13-*cis* configuration (Figure 5). This result is consistent with the observation that the hydrogen bond between the PSB and Asp97 becomes stronger after isomerization to the 13-*cis* state (see Table 1).

A similar analysis has also been performed for the water molecules, which participate in the hydrogen bonding network between the PSB and the complex counterion (Figure 6). The water W1 bridges Asp97 and Asp227 and interacts also with His75. The dynamical trajectory of 2 ps shows that these hydrogen bonds are quite stable. The VDOS computed for the water W1 in the all-*trans* state indeed shows a stretching band in the range 2300-2800 cm^{-1}, indicative of a strongly hydrogen bonded water. In contrast, the water W3, which is seen to be more mobile, presents a stretching band located at much higher frequencies in the range 3200-3550 cm^{-1}. The stretching band of W2 is somewhat in between those of W1 and W3, in the range 3000-3500 cm^{-1}. These features observed in the vibrational spectrum of the all-*trans* state are overall conserved also in the 13-*cis* state. The main

difference is observed in the spectrum of the water W1, which develops a second band around 3500 cm^{-1}. The high frequency band of W3 becomes narrower and centred around 3500 cm^{-1}, possibly reflecting the fact that this water in the 13-*cis* has a weaker hydrogen bonding interaction with the W2 (see also Table 1).

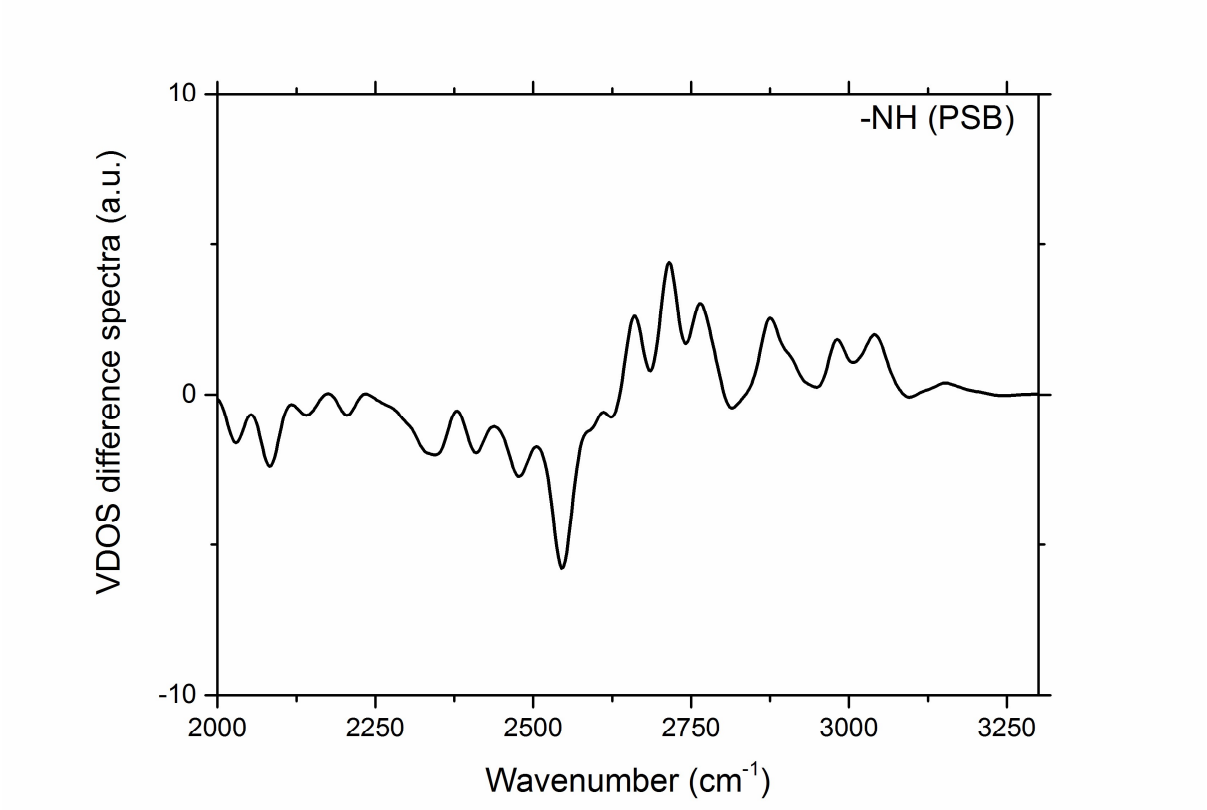

Figure 5: VDOS difference spectrum calculated by subtracting the 13-*cis* configuration from the all-*trans* configuration for our model of the native retinal A1 binding pocket. The spectra are obtained by selecting only the trajectory of the N and H atoms of the Schiff base.

Another feature of the VDOS of water molecules, common to both states before and after isomerization, is a band in the range 1490-1660 cm^{-1} that can be associated to the bending mode. Overall W1 and W2 behave differently from W3. In the 13-*cis* configuration W1 and W2 go to more intermediate, partly weak strength H-bonding with strong OH bending, while W3 now shows a tendency to stronger H-bonding (somewhat stronger interaction with Asp97 and His75), with little OH bending.

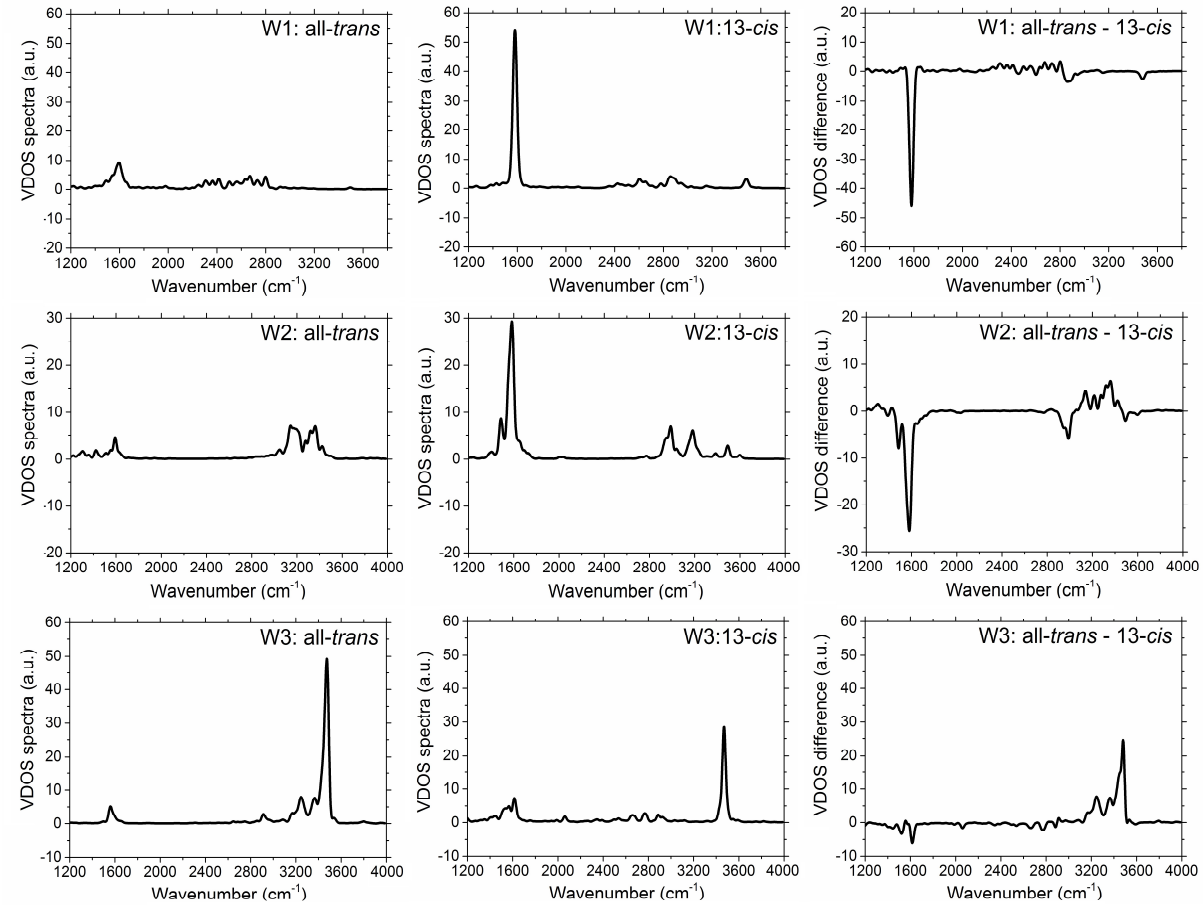

Figure 6: VDOS computed for each of the three water molecules included in our model of the native retinal A1 binding pocket. Left panels: all-*trans* configuration; Middle panels: 13-*cis* configuration; Right panels: difference spectrum calculated by subtracting the 13-*cis* configuration from the all-*trans* configuration.

Conclusions

In this work, we have investigated the structural, optical and dynamical properties of the active site of green proteorhodopsin. A fully quantum-mechanical model of the binding pocket is constructed including the retinal A1 chromophore and nearby residues, which are expected to have an important role in defining the optical properties of the system. In line with previous experimental evidence, we have found that three water molecules located in the proximity of the complex counterion form a hydrogen-bonding network, which is crucially important for stabilizing the proton on the Schiff base. TDDFT calculations show that this model is able to accurately reproduce the absorption properties of the GPR system with the native retinal A1 and the spectral modulation induced by retinal analogues. These results further validate the structural model. Finally, AIMD simulations provide some insight into changes in the vibrational modes and the rearrangement of the hydrogen-bonding network induced by the photoisomerization. It is very encouraging that our minimal model can already quite

accurately reproduce main absorption peaks. This is probably related to the relatively neutral character of the rest of the binding pocket. Therefore this minimal model can be used as a reliable starting point for future QM/MM embedding studies. These studies would offer the challenging prospects, that upon expanding the binding pocket with additional residues, it should become possible to predict *in silico* which substitutions in such residues could substantially affect the spectral properties of the system, and eventually even how this would affect stability, photo-isomerization and proton-transfer.

Acknowledgements

The use of supercomputer facilities was sponsored by NWO Physical Sciences, with financial support from the Netherlands Organization for Scientific Research (NWO). This work is dedicated to Professor Volker Buss on the occasion of his 75th anniversary in consideration of his pioneering work in computational chemistry.

Supporting Information:

Cartesian coordinates of the optimized geometries for all the investigated models. Comparison of the optimized geometries of the all-*trans* and 13-*cis* configurations for the model of the binding pocket of native GPR. TDDFT results for all the retinal analogues in comparison with experimental spectra. Comparison between B3LYP and CAM-B3LYP results.

References

(1) Bamann, C.; Bamberg, E.; Wachtveitl, J.; Glaubitz, C. Proteorhodopsin. *Biochim. Biophys. Acta BBA - Bioenerg.* **2014**, *1837*, 614–625.

(2) Béjà, O.; Aravind, L.; Koonin, E. V.; Suzuki, M. T.; Hadd, A.; Nguyen, L. P.; Jovanovich, S. B.; Gates, C. M.; Feldman, R. A.; Spudich, J. L.; et al. Bacterial Rhodopsin: Evidence for a New Type of Phototrophy in the Sea. *Science* **2000**, *289*, 1902–1906.

(3) Brown, L. S. Eubacterial Rhodopsins — Unique Photosensors and Diverse Ion Pumps. *Biochim. Biophys. Acta BBA - Bioenerg.* **2014**, *1837*, 553–561.

(4) Man, D.; Wang, W.; Sabehi, G.; Aravind, L.; Post, A. F.; Massana, R.; Spudich, E. N.; Spudich, J. L.; Béjà, O. Diversification and Spectral Tuning in Marine Proteorhodopsins. *EMBO J.* **2003**, *22*, 1725–1731.

(5) Kralj, J. M.; Spudich, E. N.; Spudich, J. L.; Rothschild, K. J. Raman Spectroscopy Reveals Direct Chromophore Interactions in the Leu/Gln105 Spectral Tuning Switch of Proteorhodopsins. *J. Phys. Chem. B* **2008**, *112*, 11770–11776.

(6) Ganapathy, S.; Bécheau, O.; Venselaar, H.; Frölich, S.; Steen, J. B. van der; Chen, Q.; Radwan, S.; Lugtenburg, J.; Hellingwerf, K. J.; Groot, H. J. M. de; et al. Modulation of Spectral Properties and Pump Activity of Proteorhodopsins by Retinal Analogues. *Biochem. J.* **2015**, *467*, 333–343.

(7) Ganapathy, S.; Venselaar, H.; Chen, Q.; de Groot, H. J. M.; Hellingwerf, K. J.; de Grip, W. J. Retinal-Based Proton Pumping in the Near Infrared. *J. Am. Chem. Soc.* **2017**, *139*, 2338–2344.

(8) Luecke, H.; Schobert, B.; Stagno, J.; Imasheva, E. S.; Wang, J. M.; Balashov, S. P.; Lanyi, J. K. Crystallographic Structure of Xanthorhodopsin, the Light-Driven Proton Pump with a Dual Chromophore. *Proc. Natl. Acad. Sci.* **2008**, *105*, 16561–16565.

(9) Ran, T.; Ozorowski, G.; Gao, Y.; Sineshchekov, O. A.; Wang, W.; Spudich, J. L.; Luecke, H. Cross-Protomer Interaction with the Photoactive Site in Oligomeric Proteorhodopsin Complexes. *Acta Crystallogr. D Biol. Crystallogr.* **2013**, *69*, 1965–1980.

(10) Gerwert, K.; Freier, E.; Wolf, S. The Role of Protein-Bound Water Molecules in Microbial Rhodopsins. *Biochim. Biophys. Acta BBA - Bioenerg.* **2014**, *1837*, 606–613.

(11) Furutani, Y.; Kandori, H. Hydrogen-Bonding Changes of Internal Water Molecules upon the Actions of Microbial Rhodopsins Studied by FTIR Spectroscopy. *Biochim. Biophys. Acta BBA - Bioenerg.* **2014**, *1837*, 598–605.

(12) te Velde, G.; Bickelhaupt, F. M.; Baerends, E. J.; Fonseca Guerra, C.; van Gisbergen, S. J. A.; Snijders, J. G.; Ziegler, T. Chemistry with ADF. *J. Comput. Chem.* **2001**, *22*, 931–967.

(13) Guerra, C. F.; Snijders, J. G.; Velde, G. te; Baerends, E. J. Towards an Order-N DFT Method. *Theor. Chem. Acc.* **1998**, *99*, 391–403.

(14) *SCM, ADF 2013.01; Theoretical Chemistry, Vrije Universiteit, Amsterdam, The Netherlands*.

(15) Perdew, J. P.; Burke, K.; Ernzerhof, M. Generalized Gradient Approximation Made Simple. *Phys. Rev. Lett.* **1996**, *77*, 3865–3868.

(16) Grimme, S.; Ehrlich, S.; Goerigk, L. Effect of the Damping Function in Dispersion Corrected Density Functional Theory. *J. Comput. Chem.* **2011**, *32*, 1456–1465.

(17) Stephens, P. J.; Devlin, F. J.; Chabalowski, C. F.; Frisch, M. J. Ab Initio Calculation of Vibrational Absorption and Circular Dichroism Spectra Using Density Functional Force Fields. *J. Phys. Chem.* **1994**, *98*, 11623–11627.

(18) Yanai, T.; Tew, D. P.; Handy, N. C. A New Hybrid Exchange–correlation Functional Using the Coulomb-Attenuating Method (CAM-B3LYP). *Chem. Phys. Lett.* **2004**, *393*, 51–57.

(19) Tawada, Y.; Tsuneda, T.; Yanagisawa, S.; Yanai, T.; Hirao, K. A Long-Range-Corrected Time-Dependent Density Functional Theory. *J. Chem. Phys.* **2004**, *120*, 8425–8433.

(20) Car, R.; Parrinello, M. Unified Approach for Molecular Dynamics and Density-Functional Theory. *Phys. Rev. Lett.* **1985**, *55*, 2471–2474.

(21) *CPMD, Copyright IBM Corp 1990-2008, Copyright MPI Für Festkörperforschung Stuttgart 1997-2001*.

(22) Lin, I.-C.; Coutinho-Neto, M. D.; Felsenheimer, C.; von Lilienfeld, O. A.; Tavernelli, I.; Rothlisberger, U. Library of Dispersion-Corrected Atom-Centered Potentials for Generalized Gradient Approximation Functionals: Elements H, C, N, O, He, Ne, Ar, and Kr. *Phys. Rev. B* **2007**, *75*, 205131.
(23) Nosé, S. A Unified Formulation of the Constant Temperature Molecular Dynamics Methods. *J. Chem. Phys.* **1984**, *81*, 511–519.
(24) Hoover, W. G. Canonical Dynamics: Equilibrium Phase-Space Distributions. *Phys. Rev. A* **1985**, *31*, 1695–1697.
(25) Hockney, R. W. A Fast Direct Solution of Poisson's Equation Using Fourier Analysis. *J ACM* **1965**, *12*, 95–113.
(26) Réat, V.; Patzelt, H.; Ferrand, M.; Pfister, C.; Oesterhelt, D.; Zaccai, G. Dynamics of Different Functional Parts of Bacteriorhodopsin: H-2H Labeling and Neutron Scattering. *Proc. Natl. Acad. Sci. U. S. A.* **1998**, *95*, 4970–4975.
(27) Malmerberg, E.; Omran, Z.; Hub, J. S.; Li, X.; Katona, G.; Westenhoff, S.; Johansson, L. C.; Andersson, M.; Cammarata, M.; Wulff, M.; et al. Time-Resolved WAXS Reveals Accelerated Conformational Changes in Iodoretinal-Substituted Proteorhodopsin. *Biophys. J.* **2011**, *101*, 1345–1353.
(28) Hayashi, S.; Tajkhorshid, E.; Schulten, K. Structural Changes during the Formation of Early Intermediates in the Bacteriorhodopsin Photocycle. *Biophys. J.* **2002**, *83*, 1281–1297.
(29) Brown, M. F.; Heyn, M. P.; Job, C.; Kim, S.; Moltke, S.; Nakanishi, K.; Nevzorov, A. A.; Struts, A. V.; Salgado, G. F. J.; Wallat, I. Solid-State 2H NMR Spectroscopy of Retinal Proteins in Aligned Membranes. *Biochim. Biophys. Acta BBA - Biomembr.* **2007**, *1768*, 2979–3000.
(30) Sugihara, M.; Buss, V.; Entel, P.; Hafner, J. The Nature of the Complex Counterion of the Chromophore in Rhodopsin. *J. Phys. Chem. B* **2004**, *108*, 3673–3680.
(31) Touw, S. I. E.; de Groot, H. J. M.; Buda, F. Ab Initio Modeling of the Spatial, Electronic, and Vibrational Structure of Schiff Base Models for Visual Photoreceptors. *J. Phys. Chem. B* **2004**, *108*, 13560–13572.
(32) Nachimuthu, S.; Gao, J.; Truhlar, D. G. A Benchmark Test Suite for Proton Transfer Energies and Its Use to Test Electronic Structure Model Chemistries. *Chem. Phys.* **2012**, *400*, 8–12.
(33) Bergo, V. B.; Sineshchekov, O. A.; Kralj, J. M.; Partha, R.; Spudich, E. N.; Rothschild, K. J.; Spudich, J. L. His-75 in Proteorhodopsin, a Novel Component in Light-Driven Proton Translocation by Primary Pumps. *J. Biol. Chem.* **2009**, *284*, 2836–2843.
(34) Herz, J.; Verhoefen, M.-K.; Weber, I.; Bamann, C.; Glaubitz, C.; Wachtveitl, J. Critical Role of Asp227 in the Photocycle of Proteorhodopsin. *Biochemistry (Mosc.)* **2012**, *51*, 5589–5600.
(35) Pfleger, N.; Wörner, A. C.; Yang, J.; Shastri, S.; Hellmich, U. A.; Aslimovska, L.; Maier, M. S. M.; Glaubitz, C. Solid-State NMR and Functional Studies on Proteorhodopsin. *Biochim. Biophys. Acta BBA - Bioenerg.* **2009**, *1787*, 697–705.
(36) Sekharan, S. Water-Mediated Spectral Shifts in Rhodopsin and Bathorhodopsin†. *Photochem. Photobiol.* **2009**, *85*, 517–520.
(37) Strambi, A.; Coto, P. B.; Ferré, N.; Olivucci, M. Effects of Water Re-Location and Cavity Trimming on the CASPT2//CASSCF/AMBER Excitation Energy of Rhodopsin. *Theor. Chem. Acc.* **2007**, *118*, 185–191.
(38) Feng, J.; Mertz, B. Proteorhodopsin Activation Is Modulated by Dynamic Changes in Internal Hydration. *Biochemistry (Mosc.)* **2015**, *54*, 7132–7141.
(39) Schapiro, I.; Weingart, O.; Buss, V. Bicycle-Pedal Isomerization in a Rhodopsin Chromophore Model. *J. Am. Chem. Soc.* **2009**, *131*, 16–17.
(40) Birge, R. R.; Cooper, T. M.; Lawrence, A. F.; Masthay, M. B.; Zhang, C. F.; Zidovetzki, R. Revised Assignment of Energy Storage in the Primary Photochemical Event in Bacteriorhodopsin. *J. Am. Chem. Soc.* **1991**, *113*, 4327–4328.

(41) Rostov, I. V.; Amos, R. D.; Kobayashi, R.; Scalmani, G.; Frisch, M. J. Studies of the Ground and Excited-State Surfaces of the Retinal Chromophore Using CAM-B3LYP. *J. Phys. Chem. B* **2010**, *114*, 5547–5555.
(42) Wolter, T.; Welke, K.; Phatak, P.; Bondar, A.-N.; Elstner, M. Excitation Energies of a Water-Bridged Twisted Retinal Structure in the Bacteriorhodopsin Proton Pump: A Theoretical Investigation. *Phys. Chem. Chem. Phys.* **2013**, *15*, 12582–12590.
(43) Altun, A.; Yokoyama, S.; Morokuma, K. Quantum Mechanical/Molecular Mechanical Studies on Spectral Tuning Mechanisms of Visual Pigments and Other Photoactive Proteins. *Photochem. Photobiol.* **2008**, *84*, 845–854.
(44) Lenz, M. O.; Huber, R.; Schmidt, B.; Gilch, P.; Kalmbach, R.; Engelhard, M.; Wachtveitl, J. First Steps of Retinal Photoisomerization in Proteorhodopsin. *Biophys. J.* **2006**, *91*, 255–262.
(45) Neumann, K.; Verhoefen, M.-K.; Weber, I.; Glaubitz, C.; Wachtveitl, J. Initial Reaction Dynamics of Proteorhodopsin Observed by Femtosecond Infrared and Visible Spectroscopy. *Biophys. J.* **2008**, *94*, 4796–4807.
(46) Dioumaev, A. K.; Brown, L. S.; Shih, J.; Spudich, E. N.; Spudich, J. L.; Lanyi, J. K. Proton Transfers in the Photochemical Reaction Cycle of Proteorhodopsin. *Biochemistry (Mosc.)* **2002**, *41*, 5348–5358.
(47) Bergo, V.; Amsden, J. J.; Spudich, E. N.; Spudich, J. L.; Rothschild, K. J. Structural Changes in the Photoactive Site of Proteorhodopsin during the Primary Photoreaction. *Biochemistry (Mosc.)* **2004**, *43*, 9075–9083.
(48) Eyring, G.; Curry, B.; Broek, A.; Lugtenburg, J.; Mathies, R. Assignment and Interpretation of Hydrogen out-of-Plane Vibrations in the Resonance Raman Spectra of Rhodopsin and Bathorhodopsin. *Biochemistry (Mosc.)* **1982**, *21*, 384–393.
(49) B. Curry; I. Palings; A.D. Broek; J.A. Pardoen; J. Lugtenburg; R.A. Mathies. *Advances in Infrared and Raman Spectroscopy*, R.J.H. Clark and R.E. Hester.; Wiley: Heyden, 1985; Vol. 12.